Synthesis and structures of sodium containing K2-xNaxMg2(SO4)3 langbeinite phases

Trussov, Ivan; Driscoll, Laura; Male, Louise; sanjuan, maria-luisa; orera, alodia; Slater, Peter

DOI:
10.1016/j.jssc.2019.04.036

Document Version
Peer reviewed version

Citation for published version (Harvard):
Trussov, I, Driscoll, L, Male, L, sanjuan, M, orera, A & Slater, P 2019, 'Synthesis and structures of sodium containing $K_{2-x}Na_xMg_2(SO_4)_3$ langbeinite phases', *Journal of Solid State Chemistry*, vol. 276, pp. 37-46. https://doi.org/10.1016/j.jssc.2019.04.036

Accepted Manuscript

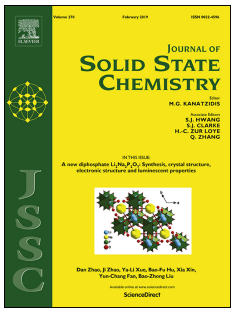

Synthesis and structures of sodium containing $K_{2-x}Na_xMg_2(SO_4)_3$ langbeinite phases

I.A. Trussov, L.L. Driscoll, L.L. Male, M.L. Sanjuan, A. Orera, P.R. Slater

PII: S0022-4596(19)30213-0

DOI: https://doi.org/10.1016/j.jssc.2019.04.036

Reference: YJSSC 20737

To appear in: *Journal of Solid State Chemistry*

Please cite this article as: I.A. Trussov, L.L. Driscoll, L.L. Male, M.L. Sanjuan, A. Orera, P.R. Slater, Synthesis and structures of sodium containing $K_{2-x}Na_xMg_2(SO_4)_3$ langbeinite phases, *Journal of Solid State Chemistry* (2019), doi: https://doi.org/10.1016/j.jssc.2019.04.036.

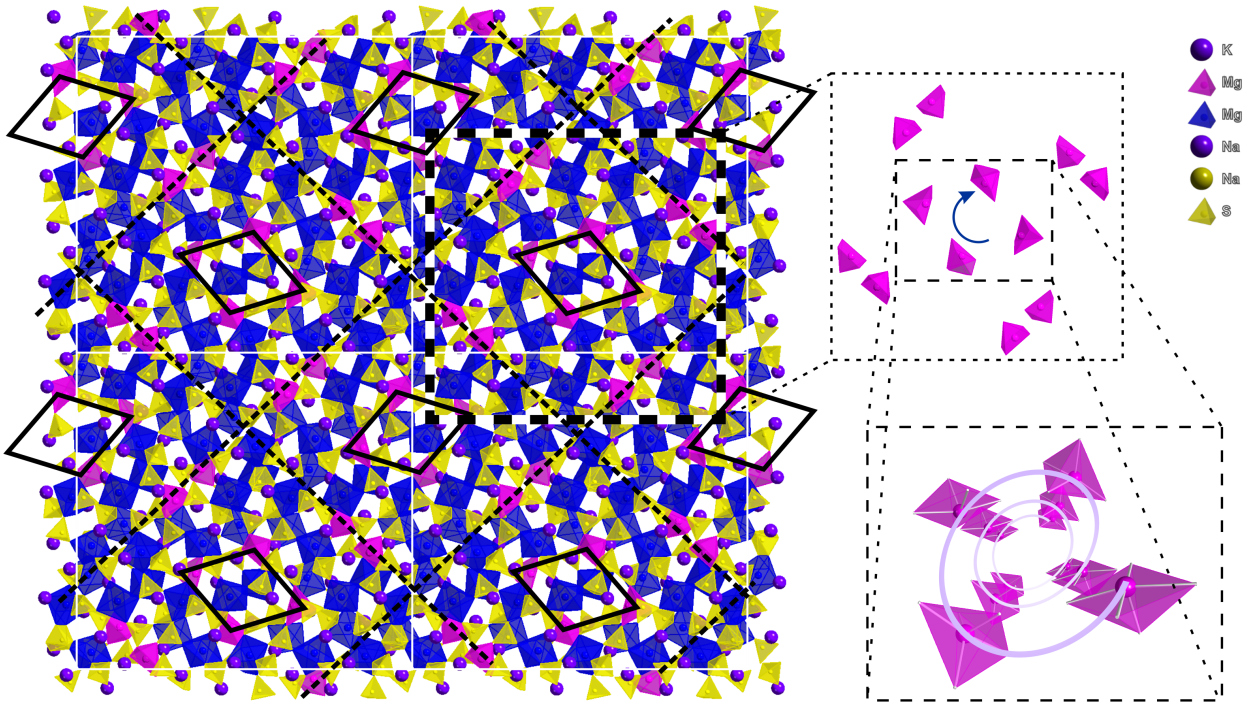

Synthesis and Structures of Sodium containing $K_{2-x}Na_xMg_2(SO_4)_3$ langbeinite phases

I. A. Trussov[1], L. L. Driscoll[1], L. L. Male[1], M. L. Sanjuan[2], A. Orera[2] and P. R. Slater[1]

[1]*School of Chemistry, University of Birmingham, Birmingham, B15 2TT, UK*

[2]*Instituto de Ciencia de Materiales de Aragón (CSIC-Universidad de Zaragoza), 50009 Zaragoza, Spain*

Abstract

In this work we report a detailed structural study of the $K_{2-x}Na_xMg_2(SO_4)_3$ series in order to evaluate the effect of Na incorporation on the structure. The results show that the cubic langbeinite structure is observed at room temperature for high Na levels; $K_{2-x}Na_xMg_2(SO_4)_3$ ($0 \leq x \leq 1.8$). Increasing the Na content further, $1.8 < x \leq 1.9$, leads to significant structural distortions, with the observation of an enlarged orthorhombic cell. These latter systems resemble a highly distorted variant of the langbeinite structure, and this relationship is also illustrated by the fact that they transform to the cubic langbeinite structure at relatively low temperature (≈200°C). In conjunction with our prior studies on $Na_2Mg_2(SO_4)_3$ (complex monoclinic cell, which also transforms to langbeinite at elevated temperature), this work highlights the flexibility of the langbeinite structure to accommodate high levels of Na ions, thus offering another potential avenue to manipulate the properties of materials with this structure-type.

Keywords: sodium magnesium sulphate, langbeinite, potassium magnesium sulphate, single crystal

1. Introduction

Materials with the langbeinite ($K_2Mg_2(SO_4)_3$) structure have attracted attention in a wide variety of areas. In geology, interest in them has principally derived from their study to help to understand sulphate planetochemistry and the formation of marine salt deposits on Earth [1]. In addition, there have been attempts to use $K_2Mg_2(SO_4)_3$ mineral for absolute dating via the $^{40}Ar/^{40}K$ method [2]. Other studies have involved investigations into thermoluminescence properties occurring in doped langbeinites[3,4]. While at room temperature, langbeinite systems show cubic symmetry, there have been reports of lowering of the symmetry to tetragonal or orthorhombic for some langbeinite-type phases at low temperature, leading to polar crystals which show ferroelectric properties [5–8]. More recently, there has been interest in the potential use of these systems as Na ion conducting electrolytes, albeit with low conductivity observed[9]. Further interest has been generated in their potential use as electrodes for Na-ion batteries. In this respect, Tarascon *et al*. have shown that $K_2Fe_2(SO_4)_3$ can be used in a Na-ion battery via electrochemical exchange of K by Na in a Na-ion conducting electrolyte, albeit the capacity was low due to the low level of exchange [10].

The original structure of langbeinite ($K_2Mg_2(SO_4)_3$) itself was studied by Zemann and Zemann in 1957[11]. It consists of a framework of corner-sharing MgO_6 octahedra and SO_4 tetrahedra, which creates large cavities in which the potassium atoms sit. The coordination of the two potassium sites differs; the K1 site is 9-coordinate while the K2 site is 12 coordinate. A close inspection of the structure shows that the larger K1 site cavity could potentially be considered as 15-coordinated if evaluated from the centre of the cavity. However, due to the fact that the K in this site is

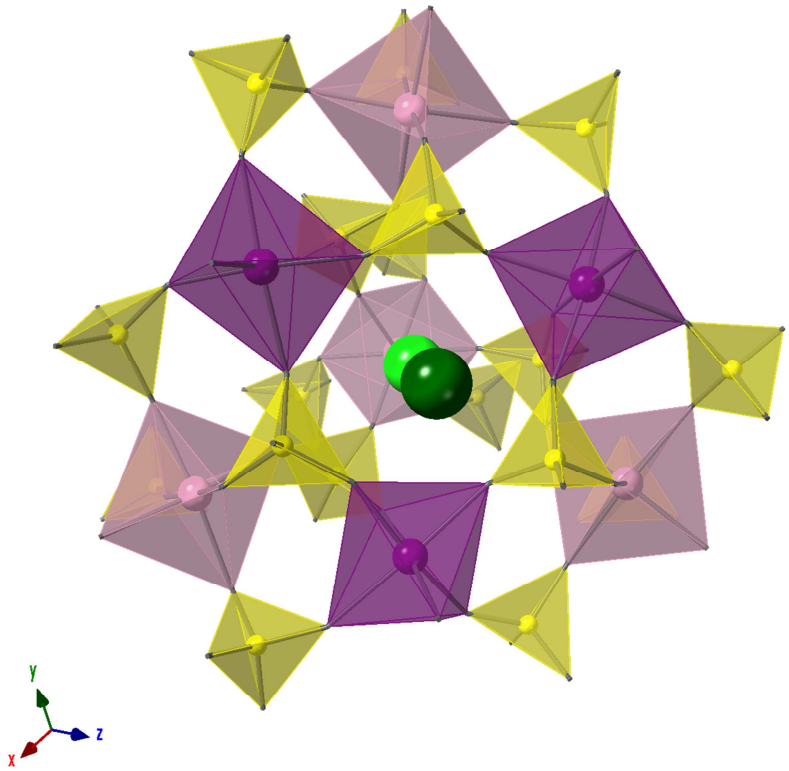

Figure 1. Langbeinite cage containing two alkali metals (green)

slightly shifted off-centre, the effective coordination is 9-coordinate. These K ion cavities form a 1-3-3-1 pattern with respect to the metal octahedra that form the general cage containing them (Figure 1); two types of metal octahedra alternate (Mg1-Mg2-Mg1-Mg2) to form the cage through corner sharing with the SO_4 tetrahedra.

Structurally the general framework of corner linked octahedra and tetrahedra shows some similarity with that of the Nasicon structure, widely studied as excellent Li/Na ion conductors[12–14]. However, while the Nasicon structure has four cavity sites within the framework, a key aspect of the langbeinite structure is the presence of only two cavity sites within the structure. The large size of these cavity sites means that the langbeinite structure favours larger alkali ions like potassium, caesium, and rubidium, while the Nasicon structure prefers smaller alkali ions such as Na, Li. Despite

this, there have been some reports of Na incorporation in langbeinite-type phase, provided that some larger cations are present to stabilise the framework, e.g. $NaBaM_2(PO_4)_3$ (M=transition metal) systems [15,16]. This would therefore suggest that it should be possible to prepare mixed K/Na langbeinite-type phase. Therefore in this work we have examined the solid solution range for $K_{2-x}Na_xMg_2(SO_4)_3$ to examine the range of Na content for which the langbeinite structure is retained. The results demonstrate a wide solid solution range and a complex structural chemistry particularly for high Na contents. In this respect, our prior work on the $Na_2Mg_2(SO_4)_3$ endmember showed that while at room temperature, the material possesses a complex monoclinic structure, there was a transition to cubic langbeinite at elevated temperatures for this phase [17]. This transition was attributed to the fact that, despite the apparent complex structure of room temperature $Na_2Mg_2(SO_4)_3$, only a small amount of rotation of the SO_4 units was required to convert it to the cubic langbeinite structure.

2. Experimental details

A range of $K_{2-x}Na_xMg_2(SO_4)_3$ ($0 \leq x \leq 1.9$) powder samples were synthesised. These were prepared via a dissolution-evaporation route used previously for the synthesis of mixed metal sulphate systems [18–20]. In this method, stoichiometric amounts of Na_2SO_4, K_2SO_4 and $MgSO_4{\cdot}7H_2O$ were dissolved in water. The solutions were then heated to evaporate the water; the resulting solid was then ground and heated at 750°C for 12 hours in air.

Single crystal samples for selected compositions across the series were grown via spontaneous crystallisation from the melt at 900°C on gold foil with a cooling rate of 0.2°C/min in air.

Powder XRD data were collected on a Panalytical Empyrean diffractometer with copper X-ray source, in reflection geometry, equipped with a Pixcel 2D detector. Variable temperature powder XRD data, up to 750^{o}C, were collected on a Bruker D8 advanced diffractometer with copper X-ray source and LynxEye detector in an Anton Paar HTK1200N furnace. Rietveld refinement using powder XRD data was performed using GSASII software[21].

For the single crystal studies, a suitable crystal was selected, mounted on glass fibre, and diffraction data were collected on an Agilent SuperNova diffractometer using an Atlas detector. The crystals were kept at 100K during data collection using an Oxford Cryosystems Cryostream. Using Olex2 [22], the structure was solved with the ShelXT[23] structure solution program using Intrinsic Phasing, and refined with the ShelXL [24] refinement package using a Least Squares approach.

Samples were also analysed by TGA-MS (Netzsch), heating at a rate of 5°C/min to 750°C in the N_2 atmosphere.

Powder samples were studied by Raman spectroscopy using the 488 nm excitation line of an Ar^{+} ion laser in a DILOR XY spectrometer with a CCD detector and approximately 2 cm^{-1} of spectral resolution. The laser output power was kept between 20 and 50 mW. The excitation and light collection were made through a 50X microscope objective lens. High temperature Raman measurements were carried out in a LINKAM TS1500V stage up to 775 °C. For measurements below RT, a SMC-TBT cryostat and liquid nitrogen were used.

3. Results and discussion

3.1. Solid solution range for $K_{2-x}Na_xMg_2(SO_4)_3$

The investigation of the effect of substitution of sodium for potassium in $K_2Mg_2(SO_4)_3$ langbeinite revealed the presence of two structural systems in the studied range. It was shown that the cubic langbeinite structure could accommodate a large amount of Na in place of K. Thus $K_{2-x}Na_xMg_2(SO_4)_3$ exhibits the cubic langbeinite structure for $0 \leq x \leq 1.8$ at room temperature (Figure 2). For higher Na levels, $1.8 < x \leq 1.9$, a new non-cubic phase, with very complex pattern, was observed. Through single crystal studies (see later), this phase was identified to be orthorhombic with a very large unit cell.

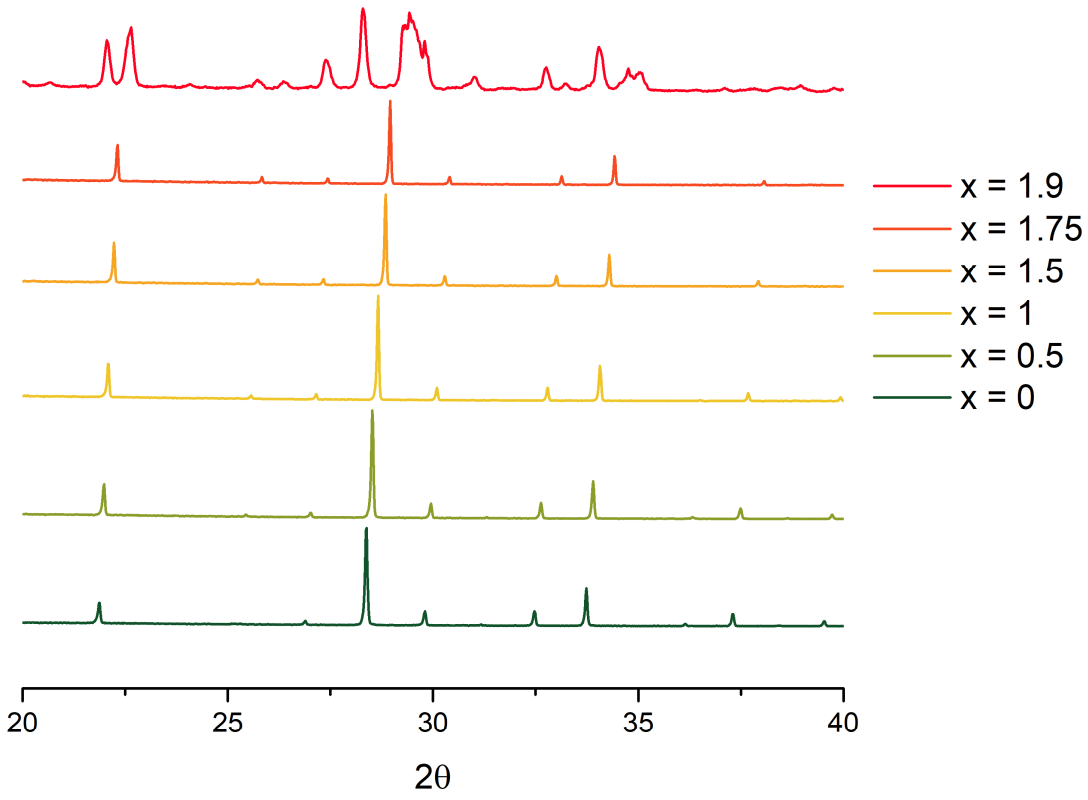

Figure 2. Powder XRD patterns for $K_{2-x}Na_xMg_2(SO_4)_3$ for $0 \leq x \leq 1.9$ at room temperature: formation of a cubic langbeinite phase for $0 \leq x \leq 1.8$, with a more complex pattern for x=1.9

Table 1. Single crystal study data

Empirical formula	$K_2Mg_2O_{12}S_3$	$K_{1.64}Na_{0.36}Mg_2O_{12}S_3$	$K_{1.33}Na_{0.68}Mg_2O_{12}S_3$	$K_{0.7}Na_{1.3}Mg_2O_{12}S_3$	$K_{0.53}Na_{1.47}Mg_2O_{12}S_3$	$K_{0.44}Na_{1.56}Mg_2O_{12}S_3$	$K_{0.23}Na_{1.78}Mg_2O_{12}S_3$	$K_{0.1}Na_{1.9}Mg_2O_{12}S_3$
Formula weight	415	409.34	404.13	394.1	391.38	389.87	386.41	384.47
Crystal system	cubic	cubic	cubic	cubic	cubic	cubic	cubic	orthorhombic
Space group	$P2_13$	$P2_13$	$P2_13$	$P2_13$	$P2_13$	$P2_13$	$P2_13$	$P2_12_12_1$
a/Å	9.89490(10)	9.86050(10)	9.82940(10)	9.75410(10)	9.74080(10)	9.72610(10)	9.71040(10)	9.56550(10)
b/Å								28.3065(3)
c/Å								30.0116(3)
Volume/Å^3	968.80(3)	958.73(3)	949.69(3)	928.03(3)	924.24(3)	920.06(3)	915.61(3)	8126.12(15)
Z	4	4	4	4	4	4	4	36
ρ_{calc}g/cm^3	2.845	2.836	2.826	2.821	2.813	2.815	2.803	2.828
μ/mm^{-1}	16.754	15.84	14.743	12.871	12.308	12.039	11.322	11.041
F(000)	824	813	802	782	777	774	767	6870
Crystal size/mm^3	0.074 × 0.044 × 0.038	0.131 × 0.105 × 0.088	0.124 × 0.096 × 0.078	0.112 × 0.079 × 0.053	0.153 × 0.111 × 0.066	0.185 × 0.144 × 0.117	0.149 × 0.068 × 0.058	0.108 × 0.08 × 0.061
2Θ range for data collection/°	12.652 to 136.378	12.696 to 149.116	12.736 to 147.712	12.836 to 148.102	12.852 to 147.302	12.872 to 147.896	12.894 to 135.594	6.906 to 147.866
Reflections collected	5285	9769	18015	8983	5222	9459	5044	77038
Independent reflections	601 [R_{int} = 0.0585, R_{sigma}=0.0239]	661 [R_{int} = 0.0310, R_{sigma} = 0.0099]	660 [R_{int} = 0.0597, R_{sigma} = 0.0126]	636 [R_{int} = 0.0436, R_{sigma} = 0.0147]	629 [R_{int} = 0.0751, R_{sigma} = 0.0285]	633 [R_{int} = 0.0305, R_{sigma} = 0.0096]	563 [R_{int} = 0.0479, R_{sigma} = 0.0196]	16241 [R_{int} = 0.0293, Rsigma = 0.0193]
Data/ restraints/ parameters	601/0/59	661/157/100	660/178/101	636/115/103	629/187/98	633/5/103	563/76/98	16241/0/1589
Goodness-of-fit on F^2	1.116	1.132	1.14	1.114	1.097	1.139	1.093	1.064
Final R indexes [I>=2σ (I)]	R_1 = 0.0183, wR_2 = 0.0484	R_1 = 0.0129, wR_2 = 0.0359	R_1 = 0.0146, wR_2 = 0.0395	R_1 = 0.0199, wR_2 = 0.0487	R_1 = 0.0282, wR_2 = 0.0743	R_1 = 0.0192, wR_2 = 0.0495	R_1 = 0.0259, wR_2 = 0.0684	R_1 = 0.0266, wR_2 = 0.0694
Final R indexes [all data]	R_1 =0.0185,wR_2=0.048	R_1 = 0.0129, wR_2 = 0.0359	R_1 = 0.0146, wR_2 = 0.0395	R_1 = 0.0203, wR_2 = 0.0490	R_1 = 0.0285, wR_2 = 0.0747	R_1 = 0.0193, wR_2 = 0.0496	R_1 = 0.0265, wR_2 = 0.0696	R_1 = 0.0288, wR_2 = 0.0710

3.2. *Structural features for $K_{2-x}Na_xMg_2(SO_4)_3$ ($0 \leq x \leq 1.8$)*

As noted earlier, $K_{2-x}Na_xMg_2(SO_4)_3$ exhibits a cubic langbeinite structure at room temperature for $0 \leq x \leq 1.8$. The cell parameters obey Vegard's Law, showing a linear decrease with increasing Na content (Figure 3), confirming a solid solution formation

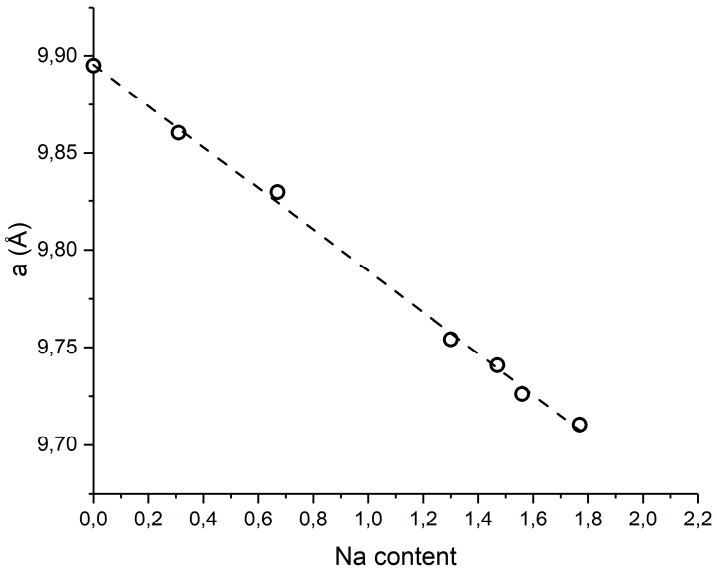

Figure 3. Cell parameters of $K_{2-x}Na_xMg_2(SO_4)_3$ (where x is 0-1.8) at 100K

across the series.

Detailed structural characterisations for selected samples across the series were performed on single crystals. These data suggest that the S-O bond lengths remain

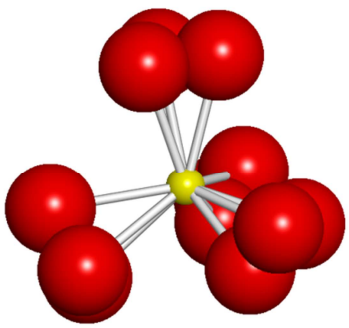

Figure 4. Rotational disorder of the SO_4 tetrahedra modelled through the use of split sites with partial occupancy

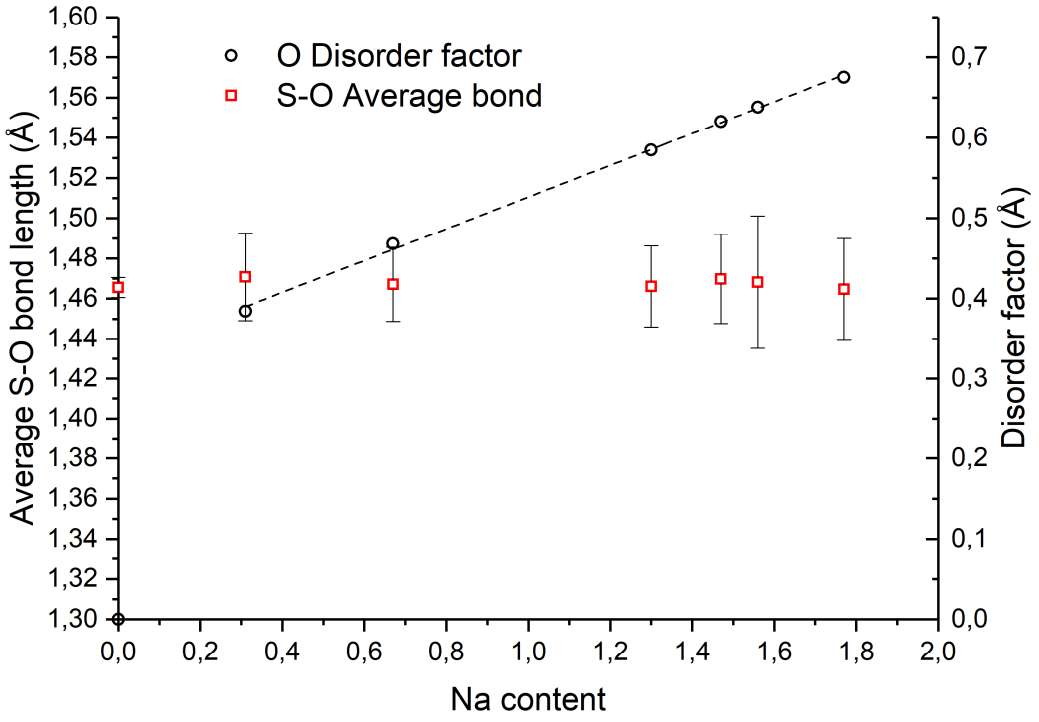

Figure 5. Variation of the "disorder factor" and average bond length of SO_4 tetrahedron with $K_{2-x}Na_xMg_2(SO_4)_3$ composition

essentially unchanged across the series with increasing of Na content. This suggests that the SO_4 unit is rigid and does not tolerate significant distortions leading to loss of tetrahedral symmetry. However, there was evidence for significant rotational disorder of the SO_4 tetrahedra, which was fitted by three split sites (Figure 4). Speer et al. reported a similar behaviour in a range of potassium containing langbeinites, where such disorder increased with increasing ionic radii of divalent cation (Zn-Co-Mn-Cd) [25]. In that previous study, the disorder was successfully modelled with prolate disk shaped thermal ellipsoids. In our case, modelling with the same strategy did not lead to a good fit to the data, and therefore the split sites approach was used. Interestingly for the $K_{2-x}Na_xMg_2(SO_4)_3$ samples studied here, this disorder does not appear in the x=0 parent phase but rather becomes more significant with increasing sodium content.

To provide a numerical measure of the rotational disorder in this system we have calculated a "disorder factor", which we define as the average separation between the

oxygen split sites. Larger values suggest the presence of more significant rotational disorder. From this calculated "disorder factor", it is clear that increasing the Na content leads to increasing disorder (Figure 5), with a strong linear dependence for this parameter versus Na content.

From the single crystal experiments, we were also able to obtain information about the separate sodium and potassium positions, showing a significant difference in the positions of sodium and potassium atoms on the same site. Potassium/sodium-oxygen environments were fitted geometrically to an ellipsoid to define the actual centre and shape of the cavities using ellipsoidal analysis of coordination polyhedra (PIEFACE software)[26]. This analysis showed that potassium (K1) is shifted off-centre of the larger cavity (axially stretched) towards the centre of the general cage and remains relatively

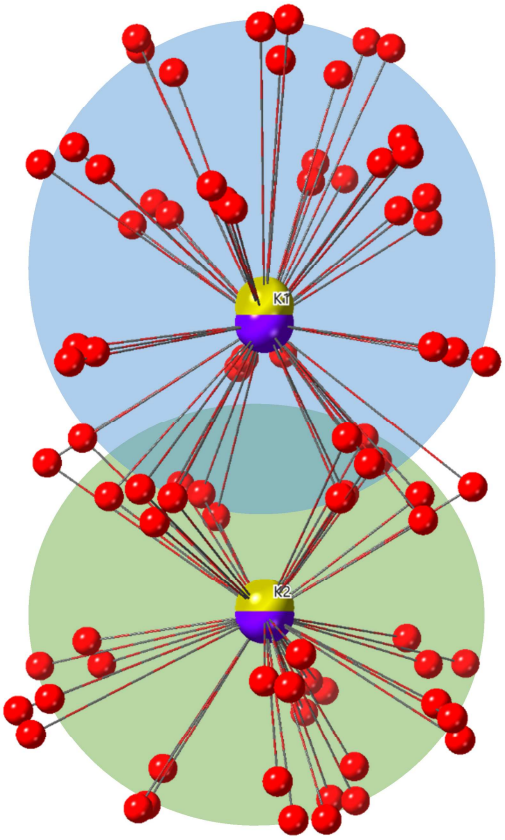

Figure 6. Langbeinite cage of $K_{0.4}Na_{1.6}Mg_2(SO_4)_3$ consisting of two cavities with off-centre displaced potassium. Blue (axially stretched) and green (axially compressed) areas are schematic representation of the ellipsoids fitted to cavities.

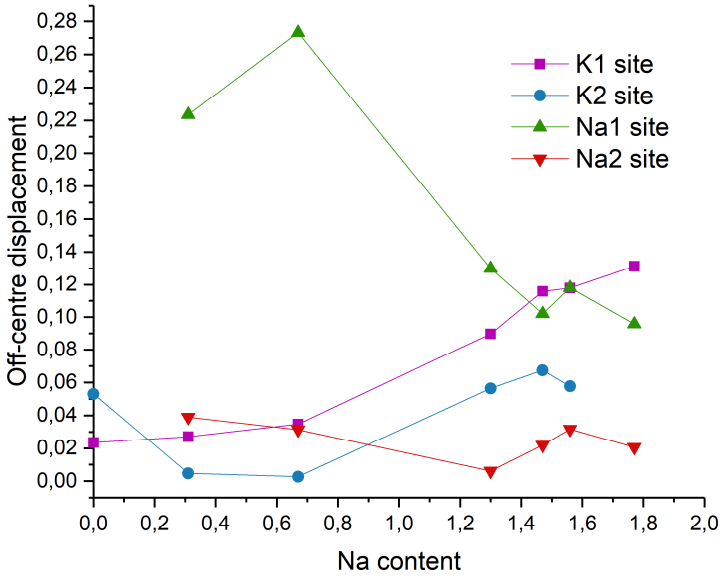

Figure 7. Potassium and sodium off-centre displacement within cavities of the cage for $K_{2-x}Na_xMg_2(SO_4)_3$

close to the centre in the smaller one (K2) (axially compressed) (Figure 6).

The size of this displacement increases as the potassium content decreases, which may explain the interesting rotational disorder of the SO_4 tetrahedra. It suggests that the cavities containing potassium have to distort to form a more spherical environment for K with similar K-O distances. For the sodium ions, the average off-centre displacement is shown to be larger (Figure 7), and increases with increasing potassium content as the unit cell expands. This increasing displacement is not surprising, as conventionally the langbeinite cavities are favoured by larger alkali metal ions. From analysis of the displacement, it can be seen that sodium tends to shift towards the wall of each cage, to allow it to be closer to those oxygen atoms and therefore achieve a more satisfactory bonding environment. These increasing off-centre displacements most likely account for the instability of sodium rich phases with respect to adopting the cubic langbeinite structure at room temperature. In particular, it is likely that local stresses result from the different cavity sizes/displacements for K/Na, and so the system reaches a point when it

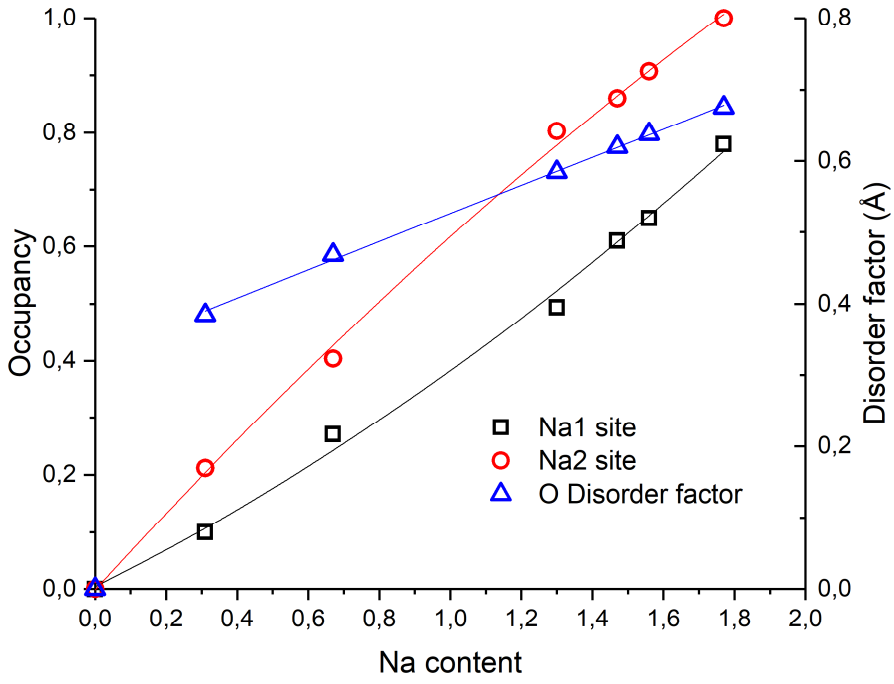

Figure 8. "Disorder factor" and sodium site occupancies for $K_{2-x}Na_xMg_2(SO_4)_3$

cannot tolerate any more stresses and so the cubic structure collapses to form the orthorhombic structure (described in the next section).

As highlighted in the introduction, there are two K sites in the langbeinite structure, and the data indicate that sodium shows some evidence of ordering between the two sites within the cell favouring the smaller Na2 site (Figure 8), while correspondingly K shows a general preference for the larger K1 site.

In view of the structural complexity of these langbeinites and the limitations of diffraction techniques, where a high number of constraints are needed in order to obtain stable refinements, we have performed Raman measurements with the aim of providing further information about the local coordination around the SO_4 groups.

Figure 9 shows the evolution of the RT Raman spectrum of the $K_{2-x}Na_xMg_2(SO_4)_3$ series with composition in the region of the internal modes of the sulphate groups[27]. Only compounds crystallizing in the $P2_13$ cubic langbeinite phase at RT are included in the figure. Bands appearing around 460, 630, 1040 and above 1100 cm^{-1} are identified as

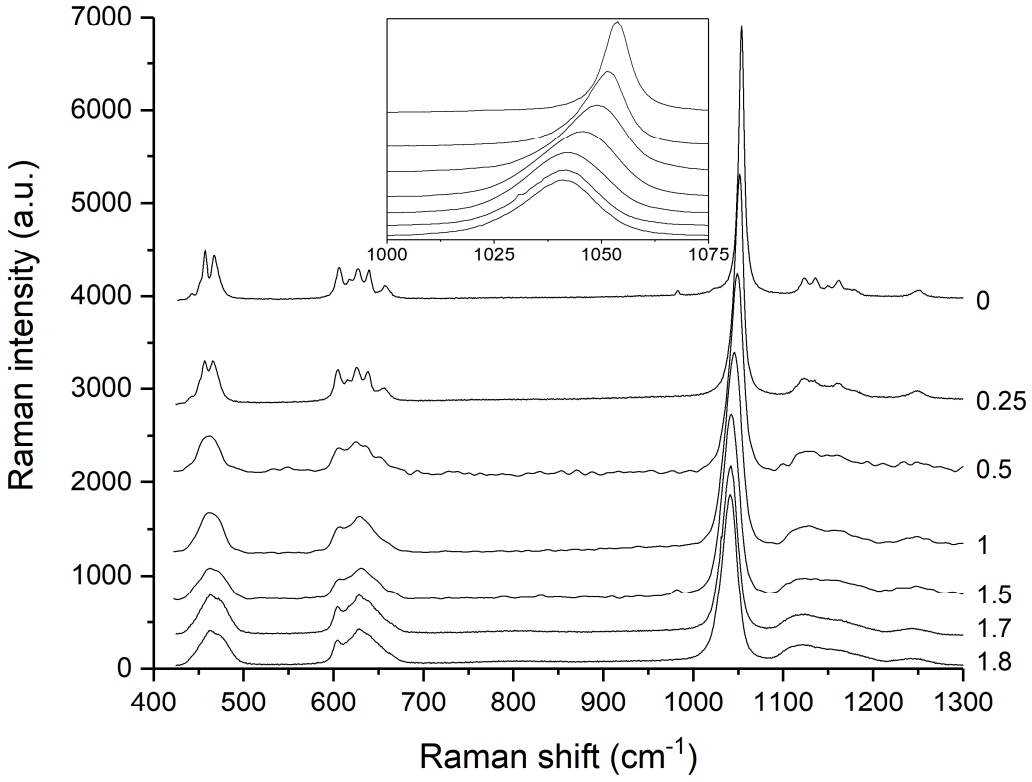

Figure 9. Raman spectra for $K_{2-x}Na_xMg_2(SO_4)_3$ at RT. The inset shows the evolution of the ν_1 band

arising from the ν_2 (symmetric bending), ν_4 (antisymmetric bending), ν_1 (symmetric stretching) and ν_3 (antisymmetric stretching) tetrahedral modes. We shall focus on the ν_1 band, whose displacements involve the symmetric breathing mode of the four oxygen atoms forming the SO_4 tetrahedron. The inset shows in detail the evolution of the ν_1 band with composition.

The band displays an unstructured aspect, as corresponds to a non-degenerate mode in a compound where all tetrahedra are crystallographically equivalent. However, a closer look highlights that this band is anomalous in several ways. First, and contrary to what would be expected according to lattice parameters, the ν_1 frequency increases with K content, suggesting shorter S-O bonds despite the lattice expansion (Figure 3). This behaviour is not uncommon: lattice expansion may result in weaker SO_4 bonding with second neighbours, and thus in a reduction of the S-O bond lengths. While the

crystallographic data suggest that the average S-O bond length appears to essentially remain constant throughout the series, the obtained structure showed quite large anisotropic atomic displacement parameters for oxygen, so that the actual oxygen sites might be even more disordered than initially accounted for using the split sites. In that case, the possibility of lengthening of the S-O bonds with increasing Na content cannot be discarded.

Another peculiarity of the ν_1 band is its composition-dependent broadening and asymmetric shape. Figure 10 shows the total linewidth and the difference between the left and right widths as a function of K content. Among the possible sources of asymmetry in the Raman spectra we propose that in the present case it is caused by the positional disorder of oxygen and Na/K cations. Oxygen split sites are indeed expected to result in a distribution of SO_4 breathing mode frequencies, but the question arises as to what is the actual origin of this splitting. In the structural analysis, the oxygen disorder has been parameterized by the disorder factor (O-O distance between split sites) and this is seen to

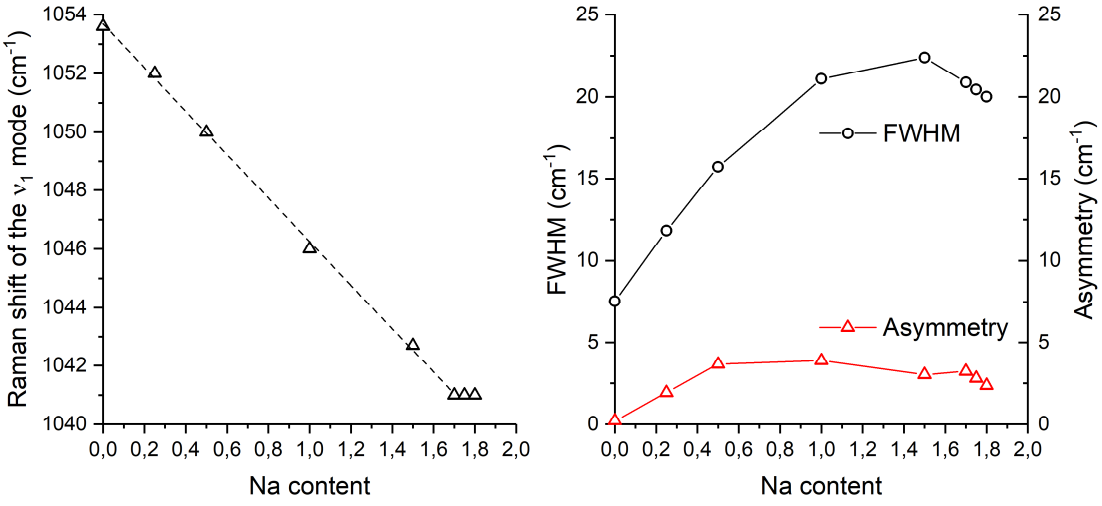

Figure 10. a) Raman shift of the ν_1 breathing mode at RT as a function of Na content in the $K_{2-x}Na_xMg_2(SO_4)_3$ series; b) Full width at half maximum (black circles) and asymmetry (red triangles) of the ν_1 breathing mode at RT as a function of Na content in the $K_{2-x}Na_xMg_2(SO_4)_3$ series. The asymmetry is defined as the difference between the left and right half widths.

increase with Na content. Similarly, the linewidth of the ν_1 band increases towards the Na rich side with a maximum around [Na] = 1.5. We note that remarkable broadening is also observed for $Na_2Mg_2(SO_4)_3$ in its high temperature cubic langbeinite-type phase[17]. Thus, it seems likely that the positional disorder of Na ions is the main cause of broadening and asymmetry, with a smaller contribution of chemical disorder required to explain the presence of a maximum as a function of K/Na content. At this point we note that different coordinates were refined for Na and K atoms sharing sites, which suggests that local displacements may occur because of the large size of the (Na, K) cavities in the langbeinite structure, and that these displacements will be different for Na and K cations. Then, Na ions might be closer to the SO_4 tetrahedra than assumed, implying local O shifts toward the nearby Na atoms thus resulting in longer S-O distance and in site-splitting. Broadening and asymmetry, therefore, reflect the instability of the cubic langbeinite structure at room temperature, as the amount of the smaller Na cations is increased.

Variable temperature spectra of Na-rich members of the series with cubic symmetry at RT were recorded down to 77K with a twofold purpose: first, despite the fact that single crystal XRD at 100K does not show evidence of symmetry lowering for Na content below x = 1.9, we thought that Raman scattering might unveil local structures

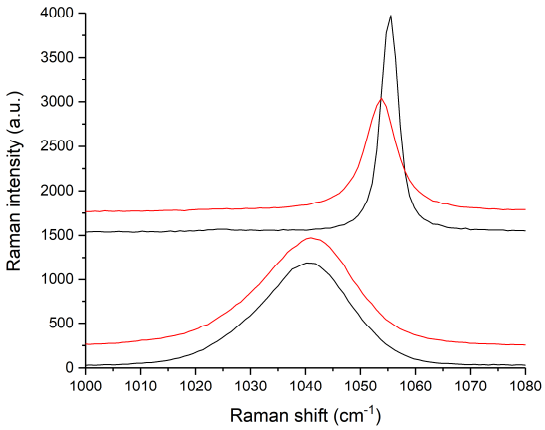

Figure 11. ν_1 band of $K_{0.2}Na_{1.8}Mg_2(SO_4)_3$ (lower graphs) and of $K_2Mg_2(SO_4)_3$ (upper graphs) at RT (in red) and 77K (in black)

preluding to a change to orthorhombic symmetry for $K_{0.2}Na_{1.8}Mg_2(SO_4)_3$. The second goal was to see, in the event that no phase transition occurs, whether minimising thermal contributions to the linewidth helps to resolve underlying components of the ν_1 band belonging to different local configurations of the SO_4 tetrahedra. The $K_2Mg_2(SO_4)_3$ endmember compound was also measured for comparison purposes. Figure 11 shows the ν_1 band of $K_{0.2}Na_{1.8}Mg_2(SO_4)_3$ and of $K_2Mg_2(SO_4)_3$ at RT and 77K. The full spectra of $K_{0.2}Na_{1.8}Mg_2(SO_4)_3$, shown in figure F1 of the supplementary material, suggest that no phase transition occurs for this composition down to 77K. With regards to the totally symmetric mode, we can see that for $K_2Mg_2(SO_4)_3$ the band narrows and hardens on cooling in a conventional way. On the contrary, for $K_{0.2}Na_{1.8}Mg_2(SO_4)_3$, the band looks essentially the same at room and low temperature: the linewidth, intensity and even the frequency remain fairly constant, and the same can be said for the rest of the spectrum (Figure F1 supplementary). This difference implies that for $K_{0.2}Na_{1.8}Mg_2(SO_4)_3$, the linewidth does not arise from the usual thermal broadening processes, neither from dynamic ones, but rather from static positional disorder, as proposed above. The non-observation of well resolved components is then attributed to the quasi-continuous distribution of O positions, which can be described by means of split sites and large thermal ellipsoids.

3.3. Structural features of $Na_{1.9}K_{0.1}Mg_2(SO_4)_3$

The structure of $Na_{1.9}K_{0.1}Mg_2(SO_4)_3$ was solved from single crystal data (see tables T1-T3 in the supplementary information for the complete structural information, CSD deposition number CCDC 1899173). It is a non-centrosymmetric orthorhombic cell with space group $P2_12_12_1$. The structure is very complex, with a very large unit cell. The unit cell consists of the SO_4 tetrahedra corner sharing with MgO_6 octahedra or MgO_5 square pyramid units, with the latter essentially highly distorted six-coordinated octahedral with

one longer bond distance (Figure 12). The average interatomic distances in the MgO_6 and the MgO_5 units are 2.031(3)Å and 1.978(2)Å respectively. The presence of MgO_5 square pyramids in sulphate crystals is not common, which is most likely due to the lower stability expected for such polar units. Here a very narrow range of bond distances and close to ideal bond valence sum +2.030(27) might explain the formation of these polar pyramids.

Despite the orthorhombic symmetry and very large unit cell, structurally the system is closely related to that of langbeinite. Indeed, it can be considered as a highly relaxed 1x3x3 superstructure of langbeinite with some distorted MgO_6 units. The origin of this complex superstructure lies in the ordering of the MgO_5 pyramids (Figure 13). The MgO_5 pyramids are combined in two types of clusters in the crystal lattice. The first type is a cluster of two square pyramids with non-parallel base-facing (double pyramid cluster). There are two orientations of this type of cluster in the unit cell forming two almost perpendicular surfaces (0 1 1) and (0 -1 1) via symmetry. Both have polarisation along the *a* axis opposite to each other. Interestingly, the 6 coordinate Mg11 site atoms, which have the largest BVS +2.24, are located at the crossing of these surfaces. This could mean that there is significant local distortion polarisation present in this region, which places a large strain on these MgO_6 units. These surfaces divide the lattice into squares with side length around 20Å. Each square contains a second type of MgO_5 cluster - a combination of four MgO_5 units in the centre of square forming a helix with total polarisation in the centre

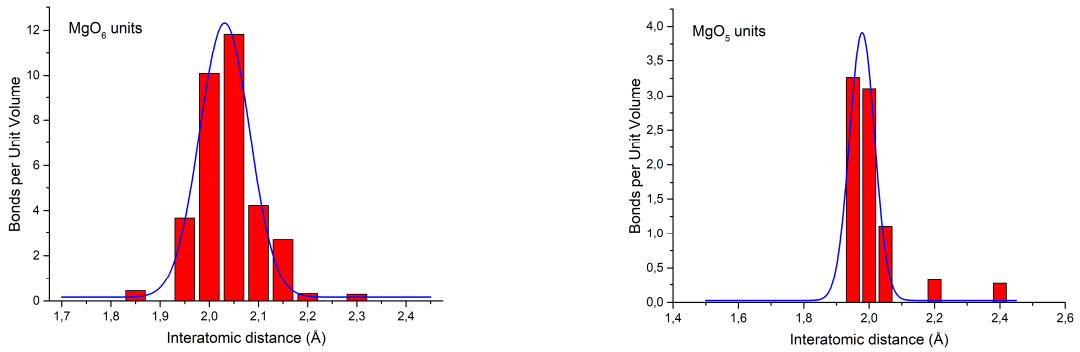

Figure 12. Distribution of bond lengths (with Gaussian fitting) for Mg sites.

directed along the axis of the helix. There are two types of helixes in the lattice located in a chequered pattern in relation to these squares. Both types have the same clockwise downwards rotation, with, however, the opposite polarisation.

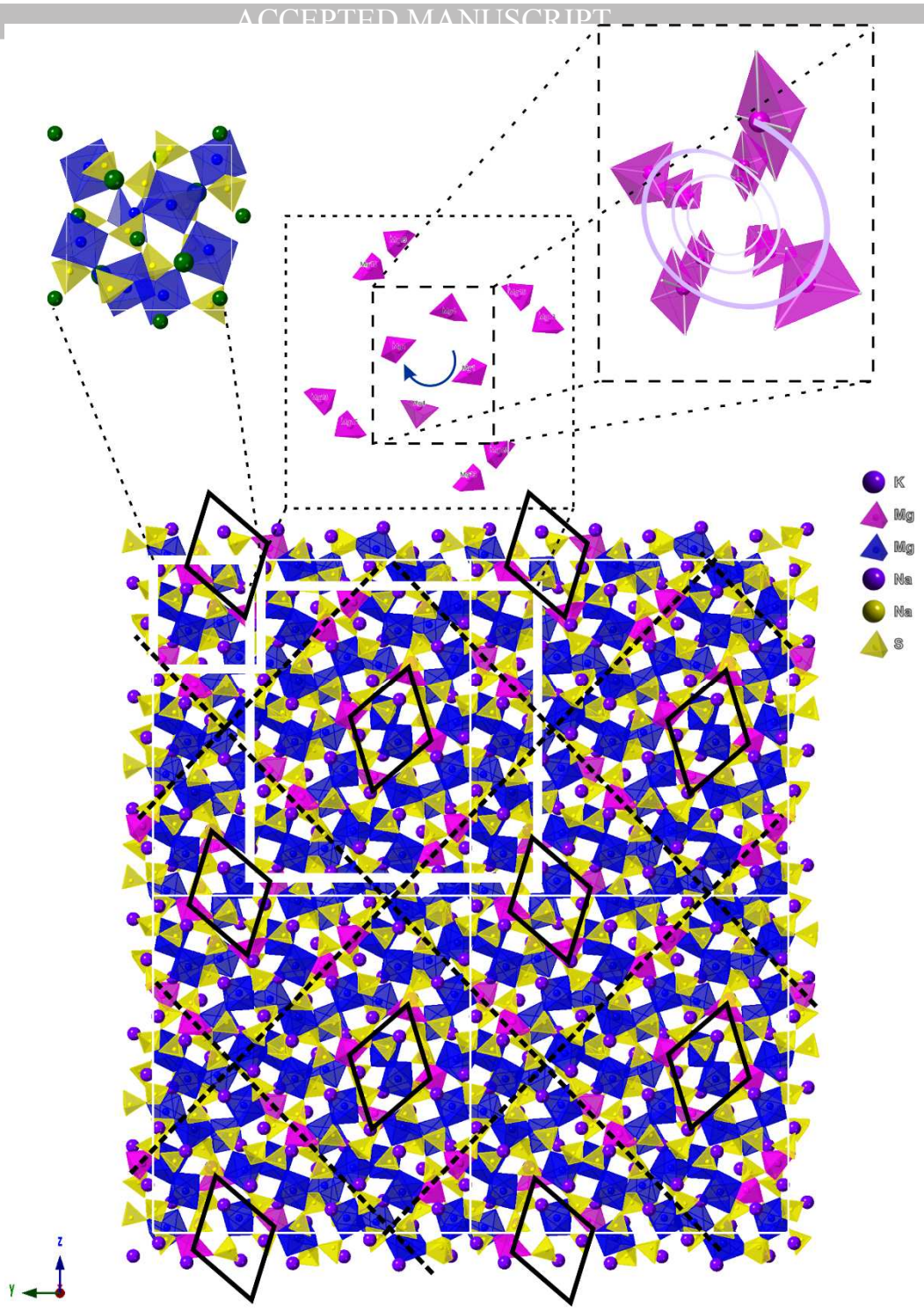

Figure 13. 2x2x2 super cell structure showing orientations of two types of helix pyramid clusters(black diamonds) separated by surfaces formed by double pyramid clusters (black dash lines) and comparison with high temperature langbeinite unit cell (top left corner) (MgO_5 pyramids are labelled pink). In the top right corner an enlarged view of the helix is shown, illustrating the spiralling of the pyramids

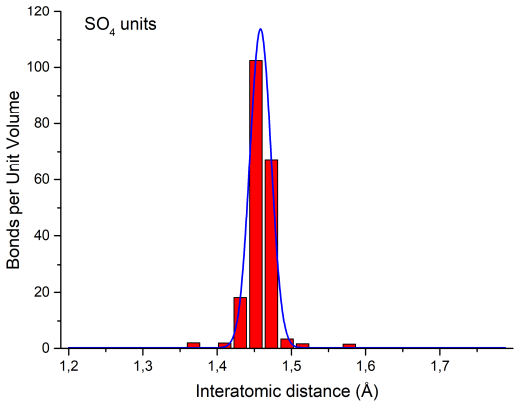

Figure 14. Distribution of bond lengths in SO_4 units with Gaussian fitting

As for the cubic langbeinite structure series, the SO_4 tetrahedra are symmetrical, with a narrow distribution of bond lengths (Figure 14), and an average S-O bond length of 1.458(1) Å. Similarly, some of the tetrahedra show evidence of rotational disorder, modelled as split sites, which could be related either to alignment of helixes and formation of an even larger supercell or to local variations in Na/K content as suggested for the cubic langbeinite series.

The cell contains 18 alkali metal sites, with only half of these containing potassium ions, with an average occupancy of ≈0.1. The other sites are only occupied by sodium (Table 2), which can be explained by the different sizes of these cavity sites.

Table 2. Na/K site occupancies for mixed alkali sites in $K_{0.1}Na_{1.9}Mg_2(SO_4)_3$. Other alkali metal sites are fully occupied by Na.

Atom	Occupancy	Atom	Occupancy	Atom	Occupancy
K1	0.116(13)	K2	0.108(12)	K4	0.110(12)
K6	0.090(12)	K9	0.104(13)	K12	0.096(12)
K13	0.110(12)	K15	0.095(11)	K18	0.115(12)
Na1	0.884(13)	Na2	0.892(12)	Na4	0.890(12)
Na6	0.910(12)	Na9	0.896(13)	Na12	0.904(12)
Na13	0.890(12)	Na15	0.905(11)	Na18	0.885(12)

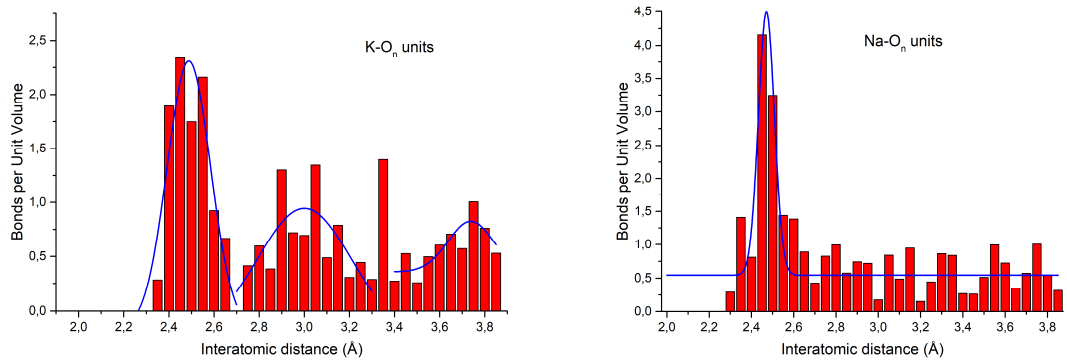

Figure 15. Distribution of interatomic distances (with Gaussian fitting) for selected potassium and sodium surroundings.

The sodium sites form a 3D chiral network with relatively high translational symmetry related to a 1x⅓x⅓ subcell unit. Sites partially occupied with potassium form the same chiral network with opposite rotation. Figure 15 shows that the distribution of the Na-O bonds for the Na only sites has a sharp peak at 2.471Å. At the same time the distribution of Na/K-O bonds for mixed sites is more complex. The figure shows the presence of more than three broad distribution peaks. These can be described as spheres of oxygen surrounding the potassium containing sites, with the first peak at 2.488 Å, second at 3.000 Å and third at 3.738Å. This may indicate that K containing cavities are larger and have lower symmetry.

At higher temperature the structure of $Na_{1.9}K_{0.1}Mg_2(SO_4)_3$ converts into the simple cubic $P2_13$ langbeinite structure (Figure 16). A similar transition was previously reported for $Na_2Mg_2(SO_4)_3$[17]. VTXRD showed that the phase transition into the cubic langbeinite structure occurs at a temperature slightly below 200°C (Figure 17), which is a lower temperature than observed for $Na_2Mg_2(SO_4)_3$. In agreement with this phase transition, the DTA curve of the TGA experiment also showed a peak at 186.2°C (Figure 17), corresponding to the phase transition. Cell volume data show a clear change at this phase transition (Figure 18), with an effective discontinuous expansion at this temperature.

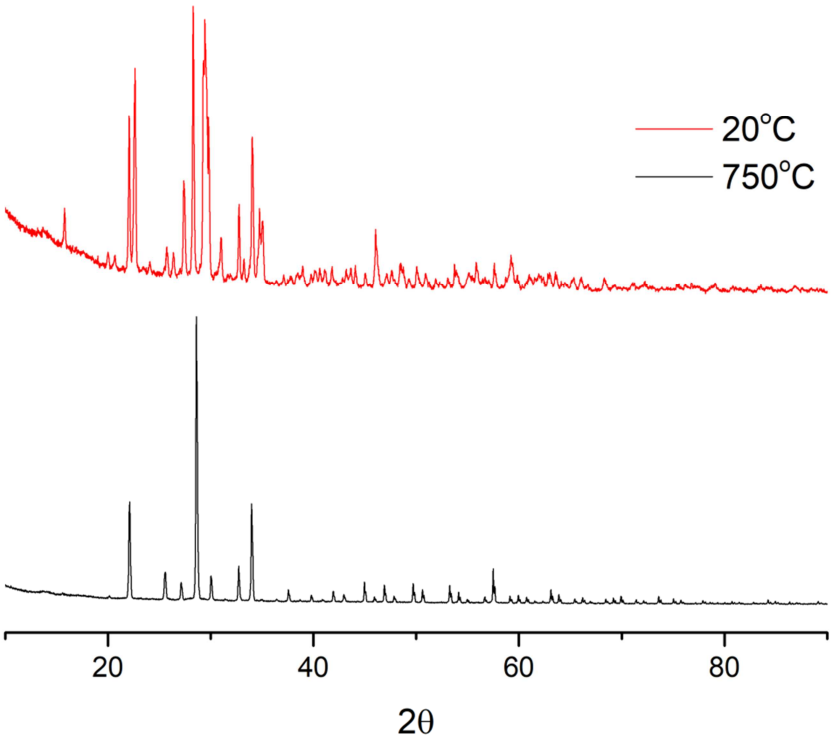

Figure 16. XRD patterns of $K_{0.1}Na_{1.9}Mg_2(SO_4)_3$ at 20°C and 750°C

Considering strong motions of ions at high temperatures and the previously described significant rotational disorder of SO_4 units in related cubic langbeinite phases at room temperatures, we assumed that in this case similar rotational disorder might be observed. Rietveld refinement using the high temperature powder diffraction data was, therefore, performed using a rigid body approach for the SO_4 unit with splitting into three tetrahedrons with partial occupancy ⅓ in order to model rotational disorder around a single sulphur atom. The size of the rigid body, i.e. S-O bond length, was allowed to refine as well. Isotropic thermal displacement parameters were constrained to be the same for all oxygen atoms, while the alkali metals were constrained to be on the same site and the site occupancy constrained to the values expected from the chemical composition.

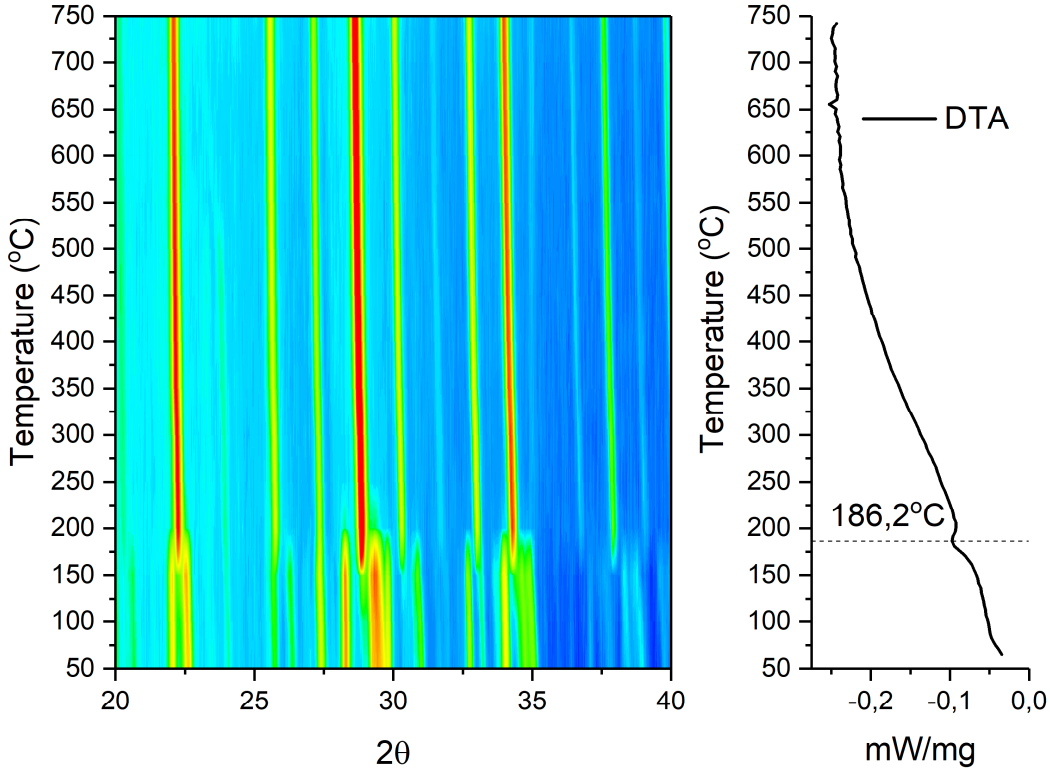

Figure 17. Contour plot of variable temperature XRD and DTA curve of $K_{0.1}Na_{1.9}Mg_2(SO_4)_3$ during the cooling stage. The results show a transition to a cubic langbeinite structure at elevated temperatures

This approach allowed us to improve the R_{wp} from ~15% down to ~10% while maintaining a sensible structural solution (Figure F2 supplementary). Further improvements to the model would require the introduction of anisotropic atomic displacement parameters, however this makes the refinement unstable due to the high number of variables and the insufficient amount of data available in powder XRD. Table T4 in supplementary contains structural information about $K_{0.1}Na_{1.9}Mg_2(SO_4)_3$ at 750°C.

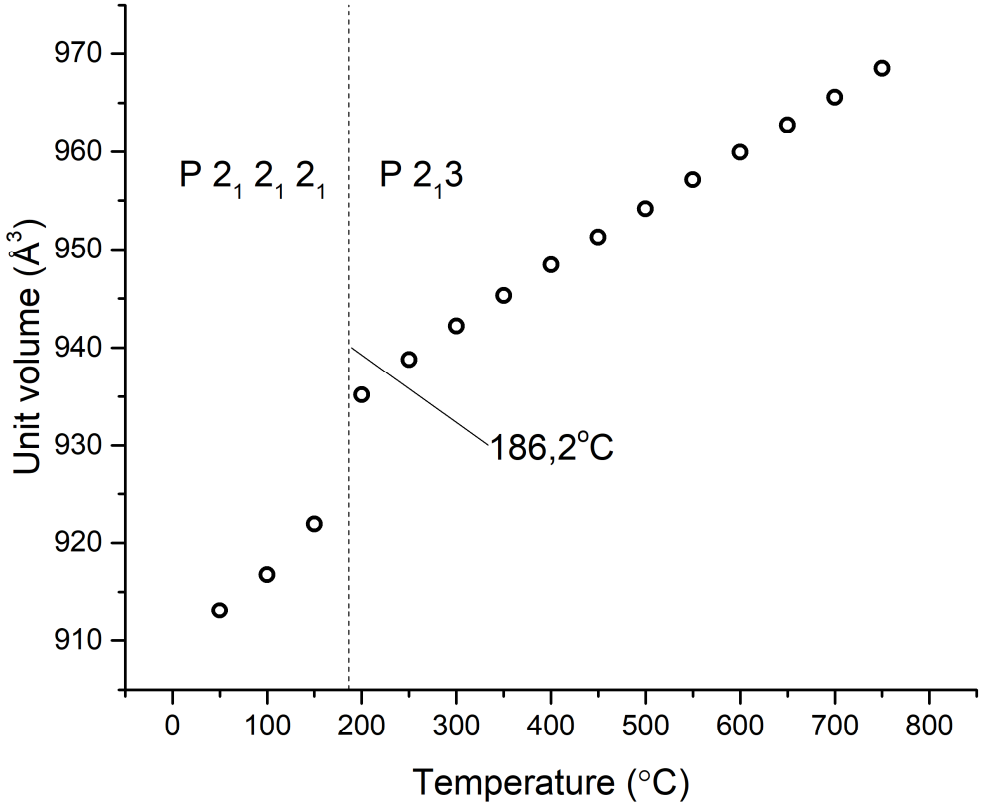

Figure 18. Unit volume of $K_{0.1}Na_{1.9}Mg_2(SO_4)_3$ versus temperature obtained from Rietveld refinement using powder VT-XRD data. The unit volume for the cubic phase is given by the volume of the unit cell, while the volume for the orthorhombic phase is taken as $^1/_9$ the overall unit cell volume.

The refined structure at 750°C suggested very large rotational distortions of the SO_4 unit, with a disorder factor in this system of up to 0.94 (Figure 19). In addition the apparent S-O bond length in the rigid body converged to a value of 1.638(4)Å. This value is much larger than expected for a sulphate group, and would suggest that there are some local displacements of the sulphur. It is particularly noteworthy that the disorder factor and apparent rigid body bond length significantly rise in value between 650 and 700°C. This could be an indication of another phase transition, although at the same time, the cell does not appear to change symmetry. There is, however, a weak feature in the DTA curve in this region (Figure 17). Fractional occupancies of sodium and potassium show the same ordering between two sites as at room temperature (potassium favours the larger cavity, while sodium the smaller).

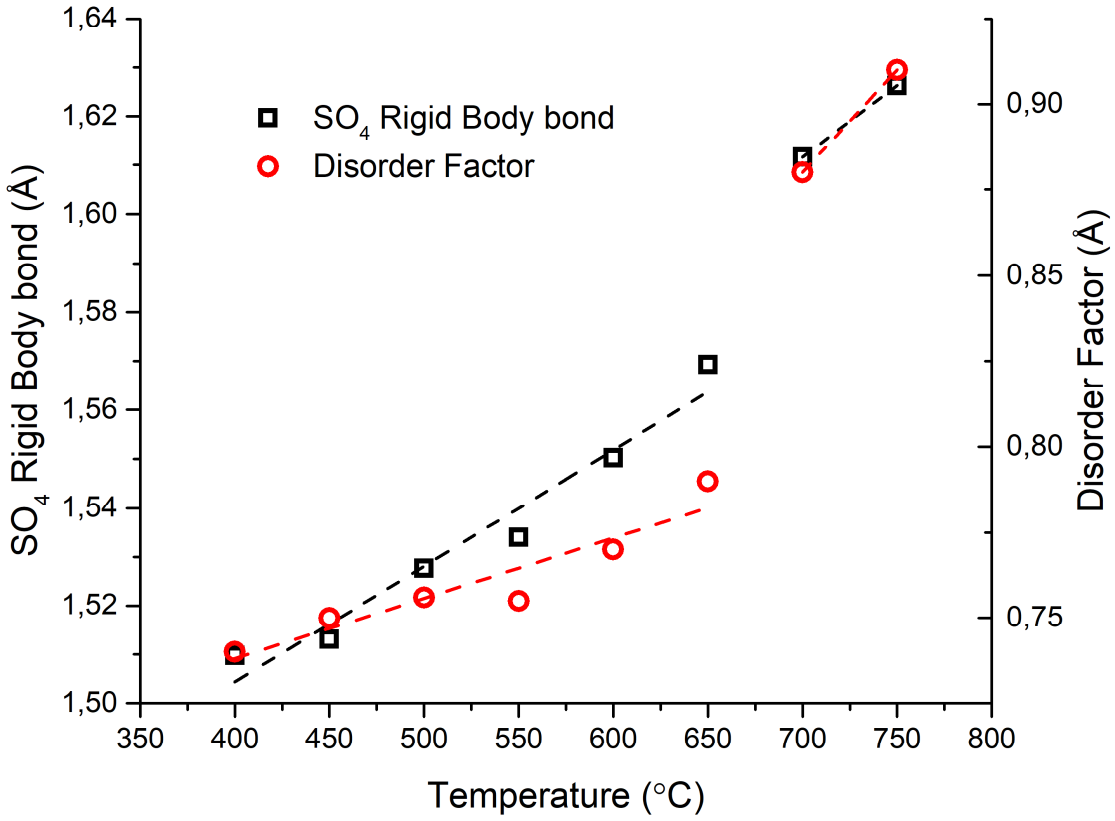

Figure 19. Rigid body Bond length and disorder factor for $K_{0.1}Na_{1.9}Mg_2(SO_4)_3$ with varying temperature.

The transition from the low temperature orthorhombic cell to high temperature cubic langbeinite can be explained by the fact that the structure of the former is similar to a 1x3x3 langbeinite supercell. Thus, the low temperature orthorhombic phase can be classed as a highly disordered variant of the langbeinite structure. While orthorhombic langbeinite phases have been previously reported below room temperature, e.g. $K_2(Ca/Cd)_2(SO_4)_3$[4,5], the orthorhombic distortion is much lower than observed for the $K_{0.1}Na_{1.9}Mg_2(SO_4)_3$ system reported here, and there was no evidence for an enlarged supercell in the former studies.

The structural evolution of $K_{0.1}Na_{1.9}Mg_2(SO_4)_3$ was also followed by Raman scattering from 77 K to 775°C (1048 K) (see the whole series of spectra in figures F3 and F4 of the supplementary material). Measurements below RT were undertaken in the search

for a possible phase transition from orthorhombic to monoclinic symmetry, similar to the one detected in our previous study on $Na_2Mg_2(SO_4)_3$ at around 100 °C [17]. As figure F3 shows, no clear evidence of new modes or of mode splitting can be ascertained, although some modes display an anomalous intensity increase that might be a hint of a nearby transition occurring perhaps below 77K. On the contrary, the phase transition to cubic symmetry is clearly observed between 150 and 200 °C, in perfect agreement with the XRD results (Figure F4 supplementary). Above 200 °C the cubic phase spectrum varies very little with increasing temperature; the observed broadening is ascribed to conventional thermal effects.

Conclusions

In this work we show that Na can be incorporated into the langbeinite phase, $K_2Mg_2(SO_4)_3$. The cubic langbeinite structure is maintained at room temperature for high Na levels; $K_{2-x}Na_xMg_2(SO_4)_3$ ($0 \leq x \leq 1.8$). For higher Na levels, $1.8 < x \leq 1.9$, an enlarged orthorhombic cell is obtained, with the structure resembling a highly distorted variant of the langbeinite structure. This relationship is also illustrated by the fact that the latter phases transform to the cubic langbeinite structure at relatively low temperature (≈200°C). The work therefore highlights the flexibility of the langbeinite structure to accommodate high levels of Na ions, thus offering another avenue to manipulate the properties of materials with this structure-type.

Acknowledgements

We would like to thank the Bolashak International Scholarship fund (PhD scholarship for Ivan Trussov) for funding. The work has been supported by the Spanish Ministerio Economía y Competitividad and Feder funds through grant MAT2016-77769R as well.

References:

[1] C.N. Alpers, J.L. Jambor, D.K. Nordstrom, P.H. Ribbe, Sulfate minerals : crystallography, geochemistry, and environmental significance, Mineralogical Society of America, Washington, DC, 2000. https://copac.jisc.ac.uk/id/8111937?style=html&title=Sulfate mineralscrystallography%2C geochemistry%2C and.

[2] I. Léost, G. Féraud, M.M. Blanc-Valleron, J.M. Rouchy, First absolute dating of Miocene Langbeinite evaporites by 40 Ar/ 39 Ar laser step-heating: [K 2 Mg 2 (SO 4) 3] Stebnyk Mine (Carpathian Foredeep Basin), Geophys. Res. Lett. 28 (2001) 4347–4350. doi:10.1029/2001GL013477.

[3] R.S. Kher, A.K. Panigrahi, S.J. Dhoble, M.S.K. Khokhar, Correlation between thermoluminescence and mechanoluminescence of gamma–irradiated Dy activated potassium and magnesium mixed sulphate, Radiat. Prot. Dosimetry. 119 (2006) 66–70. doi:10.1093/rpd/nci607.

[4] N. Mandlik, P.D. Sahare, M.S. Kulkarni, B.C. Bhatt, V.N. Bhoraskar, S.D. Dhole, Study of TL and optically stimulated luminescence of K2Ca2(SO4)3:Cu nanophosphor for radiation dosimetry, J. Lumin. 146 (2014) 128–132. doi:10.1016/J.JLUMIN.2013.09.061.

[5] S.C. Abrahams, J.L. Bernstein, Piezoelectric langbeinite-type K2Cd2(SO4)3: Room temperature crystal structure and ferroelastic transformation, J. Chem. Phys. 67 (1977) 2146. doi:10.1063/1.435101.

[6] B. Březina, M. Glogarová, New ferroelectric langbeinite Tl2Cd2(SO4)3, Phys. Status Solidi. 11 (1972) K39–K42. doi:10.1002/pssa.2210110149.

[7] V. Devarajan, E. Salje, Phase transitions in langbeinites II: Raman spectroscopic investigations of K2Cd2(SO4)3, Phys. Chem. Miner. 13 (1986) 25–30. doi:10.1007/BF00307310.

[8] A. Sakai, T. Inagaki, C. Moriyoshi, K. Itoh, Micro-Raman mapping study of the phase transition in K2Mn2(SO4)3, in: Ferroelectrics, 2002: pp. 27–32. doi:10.1080/00150190211576.

[9] A. Souamti, M. Kahlaoui, B. Mohammed, A. Diego Lozano-Gorrín, D.B.H. Chehimi, Synthesis, structural and electrochemical properties of new ytterbium-doped langbeinite ceramics, Ceram. Int. 43 (2017) 10939–10947. doi:10.1016/J.CERAMINT.2017.05.132.

[10] L. Lander, G. Rousse, D. Batuk, C. V Colin, D.A. Dalla Corte, J.-M. Tarascon, Synthesis, Structure, and Electrochemical Properties of K-Based Sulfates K 2 M 2 (SO 4) 3 with M = Fe and Cu, Inorg. Chem. 56 (2017) 2013–2021. doi:10.1021/acs.inorgchem.6b02526.

[11] A. Zemann, J. Zemann, Die Kristallstruktur von Langbeinit, K2Mg2(SO4)3, Acta Crystallogr. 10 (1957) 409–413. doi:10.1107/S0365110X57001346.

[12] P.R. Slater, C. Greaves, Neutron diffraction structural study of the nasicon-related phases LixMIIxMIII2-x(SO4)3-y(SeO4)y (MII = Mg, Ni, Zn; MIII = Al, Cr), J. Mater. Chem. 4 (1994) 1463–1467. doi:10.1039/JM9940401463.

[13] P.R. Slater, C. Greaves, Synthesis and Conductivities of Sulfate/Selenate Phases Related to Nasicon: NaxM′(II)xM″(III)2-x(SO4)3-y(SeO4)y, J. Solid State Chem. 107 (1993) 12–18. doi:10.1006/jssc.1993.1317.

[14] P.R. Slater, C. Greaves, Powder neutron diffraction study of the nasicon-related phases NaxMIIxMIII2-x(SO4)3-y(SeO4)y: MII = Mg, MIII = Fe, In, J. Mater. Chem. 4 (1994) 1469–1473. doi:10.1039/JM9940401469.

[15] I. V. Zatovsky, N.Y. Strutynska, Y.A. Hizhnyi, S.G. Nedilko, N.S. Slobodyanik, N.I. Klyui, Partial Substitution of Potassium with Sodium in the K2Ti2(PO4)3 Langbeinite-Type Framework: Synthesis and Crystalline Structure of K1.75Na0.25Ti2(PO4)3, ChemistryOpen. 7 (2018) 504–512. doi:10.1002/open.201800059.

[16] M. Hidouri, H. Jerbi, M. Ben Amara, The iron phosphate NaBaFe2(PO4)3, Acta Crystallogr. Sect. E Struct. Reports Online. 64 (2008) i51–i51. doi:10.1107/S1600536808023040.

[17] I.A. Trussov, L.L. Male, M.L. Sanjuan, A. Orera, P.R. Slater, Understanding the complex structural features and phase changes in Na2Mg2(SO4)3: a combined single crystal and variable temperature powder diffraction and Raman spectroscopy study, J. Solid State Chem. (2019). doi:10.1016/j.jssc.2019.02.014.

[18] L.L. Driscoll, E. Kendrick, K.S. Knight, A.J. Wright, P.R. Slater, Investigation into the dehydration of selenate doped Na2M(SO4)2·2H2O (M = Mn, Fe, Co and Ni): Stabilisation of the high Na content alluaudite phases Na3M1.5(SO4)3-1.5x(SeO4)1.5x(M = Mn, Co and Ni) through selenate incorporation, J. Solid State Chem. 258 (2018) 64–71. doi:10.1016/j.jssc.2017.09.025.

[19] L.L. Driscoll, A.J. Wright, P.R. Slater, Designing a facile low cost synthesis strategy for the Na–V–S–O systems, NaV(SO4)2, Na3V(SO4)3 and Na2VO(SO4)2, Dalt. Trans. 47 (2018) 13535–13542. doi:10.1039/C8DT02308E.

[20] L.L. Driscoll, E. Kendrick, A.J. Wright, P.R. Slater, Investigation into the effect on structure of oxoanion doping in Na2M(SO4)2·2H2O, J. Solid State Chem. 242 (2016) 103–111. doi:10.1016/j.jssc.2016.07.004.

[21] B.H. Toby, R.B. Von Dreele, GSAS-II: The genesis of a modern open-source all purpose crystallography software package, J. Appl. Crystallogr. 46 (2013) 544–549. doi:10.1107/S0021889813003531.

[22] O. V. Dolomanov, L.J. Bourhis, R.J. Gildea, J.A.K. Howard, H. Puschmann, OLEX2 : a complete structure solution, refinement and analysis program, J. Appl. Crystallogr. 42 (2009) 339–341. doi:10.1107/S0021889808042726.

[23] G.M. Sheldrick, SHELXT – Integrated space-group and crystal-structure determination, Acta Crystallogr. Sect. A Found. Adv. 71 (2015) 3–8. doi:10.1107/S2053273314026370.

[24] G.M. Sheldrick, Crystal structure refinement with SHELXL, Acta Crystallogr. Sect. C Struct. Chem. 71 (2015) 3–8. doi:10.1107/S2053229614024218.

[25] D. Speer, E. Salje, Phase transitions in langbeinites I: Crystal chemistry and structures of K-double sulfates of the langbeinite type M 2 + + K2(SO4)3, M + +=Mg, Ni, Co, Zn, Ca, Phys. Chem. Miner. 13 (1986) 17–24. doi:10.1007/BF00307309.

[26] J. Cumby, J.P. Attfield, Ellipsoidal analysis of coordination polyhedra, Nat. Commun. 8 (2017) 14235. doi:10.1038/ncomms14235.

[27] A. Hamilton, R.I. Menzies, Raman spectra of mirabilite, Na2SO4·10H2O and the rediscovered metastable heptahydrate, Na2SO4·7H2O, J. Raman Spectrosc. 41 (2010) 1014–1020. doi:10.1002/jrs.2547.

The structural changes on Na incorporation into $K_2Mg_2(SO_4)_3$ are identified, illustrating complex structural distortions for high Na contents.

Highlights

- The cubic langbeinite structure is obtained for high levels of Na incorporation, $K_{2-x}Na_xMg_2(SO_4)_3$ ($0 \leq x \leq 1.8$).
- For higher Na contents, $1.8 < x \leq 1.9$, significant structural distortions occurs, with the observation of an enlarged orthorhombic cell.
- These latter systems transform to the cubic langbeinite structure at relatively low temperature (≈200°C).